Journal of Manufacturing Processes 66 (2021) 595–607

Contents lists available at ScienceDirect

Journal of Manufacturing Processes

journal homepage: www.elsevier.com/locate/manpro

Ultrasonic-assisted abrasive micro-deburring of micromachined metallic alloys

A. Sravan Kumar [a,b,*], Sankha Deb [b,c], S. Paul [a,b]

[a] Machine Tools and Machining Laboratory, Mechanical Engineering Department, Indian Institute of Technology Kharagpur, West Bengal, 721 302, India
[b] Mechanical Micro-Machining Laboratory, Mechanical Engineering Department, Indian Institute of Technology Kharagpur, West Bengal, 721 302, India
[c] Flexible Manufacturing System and CIM Laboratory, Mechanical Engineering Department, Indian Institute of Technology Kharagpur, West Bengal, 721 302, India

ARTICLE INFO

Keywords:
Micro-deburring
Micromilling
Ultrasonic
Abrasive

ABSTRACT

Burr formation is a common and undesirable phenomenon in metal cutting operations, reducing the quality, accuracy, and functionality of the component. In micromachining, burrs are smaller but comparable to the feature size and are difficult to remove. Most of the traditional deburring operations cannot be applied to micromachined components without proper scaling, as the feature size on the part is very small and is prone to damage. Ultrasonic energy is widely used for part cleaning. In this study, an ultrasonic-assisted abrasive micro-deburring process using a probe sonicator has been developed to remove burrs from micromilled components on a variety of metallic alloys with a focus on burr removal, preservation of dimensional accuracy of the channels, minimisation of surface damage, and improvement in surface finish. Deburring of micromilled channels of 500 μm width on aluminium 6061, copper, Ti-6Al-4 V, and bearing steel has been conducted, and the results have been analysed. Deburring occurred due to the impact of abrasives, which were accelerated by the energy of the collapsing cavitation bubbles. Burr reduction by as much as 92 % has been achieved in a very short time of ten seconds for soft materials like Al 6061 and copper, and three to six minutes for Ti-6Al-4 V and bearing steel, without damaging the components or inducing any deterioration of dimensional accuracy. The surface roughness of channels has decreased from 8.97 nm to 6.63 nm after ten seconds deburring, resulting in a 26 % improvement in surface finish.

1. Introduction

In mechanical machining operations, undesired projections of material appear due to plastic deformations termed as burrs. A burr is defined as a projection of undesired material beyond the desired machined features [1]. Burrs not only reduce the accuracy of parts — thereby affecting the mechanical properties, functionality of the components, and subsequent assemblies — but also increase the production cost. Deburring is performed as a post-machining operation, further increasing the production time and cost. In mechanical micromachining operations like micromilling, burrs are smaller than in conventional milling, but the relative size of the burrs to the size of the components is large [2–4]. This is mainly due to the dominance of ploughing, rubbing, and plastic deformation in the material removal process [3] arising as a result of size effects at the micro-scale [4]. These burrs cause problems in inspection, assembly, automation, and operation of these precision components [5], further increasing the need for burr removal in precision components.

Numerous studies have been conducted on burr formation [6–14], burr minimization [8,12,14–18], and deburring in conventional machining operations. The most commonly used deburring processes in the industry are batch deburring methods like rotating brush, barrel deburring, abrasive deburring, water jet deburring, and electrochemical deburring [8]. These techniques, without proper scaling, are not suitable for the removal of burrs in micromachined parts as the feature size in these components is very small and can be distorted by these deburring operations. Hence, burr formation in micromilling is a more serious issue as compared to conventional milling.

Sufficient research exists on the burr formation in micromilling of different materials [2–4,19–25], but less literature is available on the deburring of micromilled components. Lee and Dornfeld [19] have studied the burr formation in micromilling of ductile materials like

* Corresponding author at: Machine Tools and Machining Laboratory, Mechanical Engineering Department, Indian Institute of Technology Kharagpur, West Bengal, 721 302, India.

E-mail addresses: asravan.kumar@outlook.com, sravan.ammiraju@iitkgp.ac.in (A.S. Kumar).

https://doi.org/10.1016/j.jmapro.2021.04.019
Received 1 December 2020; Received in revised form 4 April 2021; Accepted 9 April 2021
Available online 30 April 2021
1526-6125/

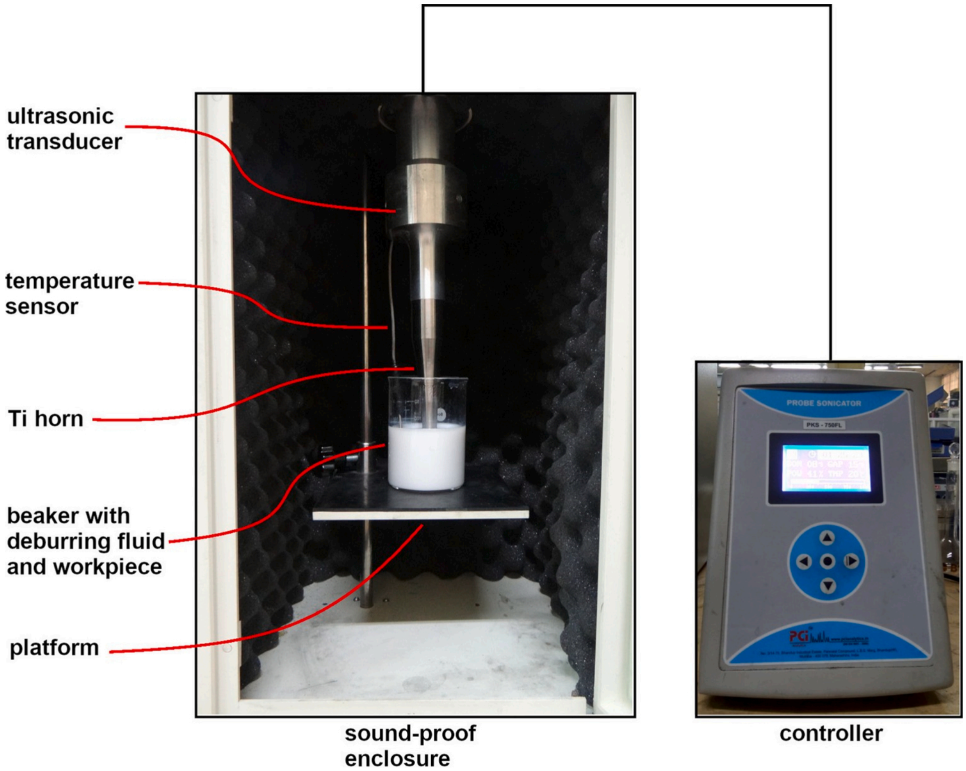

Fig. 1. Ultrasonic-assisted abrasive micro-deburring setup showing the main components.

aluminium and copper. They have reported that the majority of burrs formed in micromilling were top burrs, and these are considered to be the most difficult to remove. Filiz et al. [20] have conducted a parametric study on the micromilling of copper and have observed that burr size is smaller at higher feed rates. Hassanpour et al. [22] have undertaken micromilling of Ti-6Al-4 V alloy and have reported that by increasing the cutting speed, the material plastic strain rate is increased and has lead to a reduction in burr size. Vazquez et al. [23] have studied the effect of different cooling and lubricating conditions on the micromilling of Ti-6Al-4 V alloy and concluded that minimum quantity lubrication (MQL) with jet oriented against the feed direction resulted in minimum top burrs. Saptaji and Subbiah [26] have evaluated the use of tapered micromilling tools with taper angle varying from 15° to 50° to machine microchannels on aluminium 6061. They have reported that burr-free micro-features can be generated for mould-making using tapered tools, and the moulds showed good performance during de-embossing in hot embossing operations using PMMA. Attempts were also made to generate smaller burrs using ultrasonic-assisted micromilling technique [27–29]. Reduction in burr height was achieved during milling by using ultrasonic vibrations. However, complete burr removal could not be achieved over a wide process parameter range. The above studies have reported the minimization of burr formation in micromilling of different materials. However, complete removal of burr could not be achieved, establishing the need for deburring operation post-machining.

Several deburring techniques from various categories like mechanical deburring, thermal deburring, electrochemical deburring, and ultrasonic-assisted deburring methods have been documented in literature [30,31]. Jeong et al. [32] have studied the application of micro-EDM process for deburring micro-features on conductive materials. They have reported that by using micro-EDM, selective material removal can be achieved at the burrs without causing any collateral damage. Mathai and Melkote [33] have evaluated the deburring of 500 μm micromilled grooves on copper and tool steel using abrasive assisted brush deburring with SiC and diamond grits. They have reported successful deburring of the grooves but with an increase in the edge radius. Liao et al. [34] have developed a dual-purpose tool for polishing and deburring parts. They have developed a tool control scheme and reported that uniform polishing and deburring could be achieved by controlling the tool head pressure and length. Malayath et al. [35] have performed simultaneous milling and deburring of microchannels on PMMA and OHFC copper using carbonyl iron particles (CIP). They have concluded that the process removes micro-burrs effectively and also reduces the surface roughness provided the rotational speed of the tool is low and the flute size of the tool is larger than the size of the CIP. Okada et al. [36] demonstrated micro-deburring on Ti-6Al-4 V and tool steel using large-area electron beam (EB) radiation. They have reported that batch deburring of several small holes generated by micro-EDM could be done using this method. Balasubramaniam et al. [37] have investigated the use of abrasive jet machining for deburring stainless steel. They have reported that the abrasive jet was effective at deburring but also removed some amount of the work material. Chang et al. [38] have demonstrated laser deburring of micro-burrs generated on microchannels in a microfluidic injection mould. They have reported that the laser process can not only remove burrs but also improve the surface finish of the microchannel.

Ultrasonic energy has been widely used for cleaning components [39]. Ultrasonic cleaning uses high-frequency sound waves with a frequency above 20 kHz to remove contaminants from parts immersed in aqueous media [40]. Yeo et al. [41] have reported the use of ultrasonic cavitation energy for deburring thick metallic and non-metallic burrs. They have primarily used a bath sonicator filled with water and alumina abrasive particles for deburring and demonstrated that both metallic and non-metallic burrs could be removed by cavitating the water column in the sonicator. They have qualitatively demonstrated the deburring capability of the setup but did not conduct a quantitative study about the material removed during deburring. Horsch et al. [42] have compared the effectiveness of dry micro-peening and ultrasonic wet peening (using ultrasonic cavitation bubbles) on the deburring micro mould inserts. They have reported that the ultrasonic wet peening

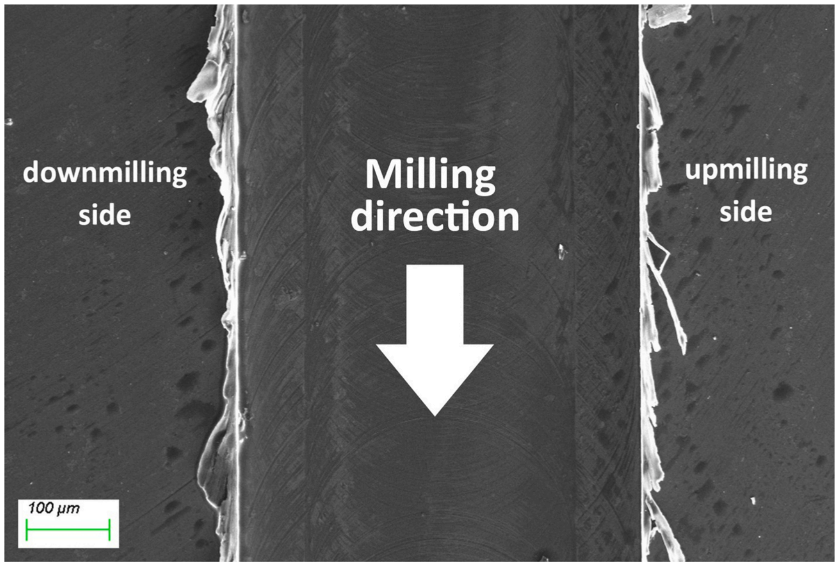

Fig. 2. SEM image of a microchannel milled on Al 6061 showing the milling direction, downmilling and upmilling sides on the top edge of the channel.

process allows for a reliable deburring of micromilled structures. However, a large peening time of up to seven hours was reported, and complete deburring and the best surface quality were reported to be achieved at different peening times, meaning a compromise between the two has to be found based on the application. Kienzler et al. [43] have done a comparison study of micromilling strategy, abrasive jet deburring, and ultrasonic wet peening for burr removal. They have concluded that ultrasonic wet peening showed the best results for deburring and have suggested that a combination of the processes can improve the surface quality. Khmelev et al. [44] have reported the use of ultrasonic cavitation bubbles in abrasive suspension and chemically active media for deburring of metals. They have reported a long deburring time (more than two hours) for effective deburring. Choi et al. [45] have studied the ultrasonic deburring of drilling burrs on aluminium using probe sonicator and abrasives. They have reported that the surface integrity and deburring effect are better when abrasives were used as compared to pure water cavitation.

The above literature survey has suggested various methods for deburring micromachined components. Various objectives were fulfilled in different individual studies. But all the objectives could not be achieved in the same study. In this paper, an ultrasonic-assisted abrasive micro-deburring method employing a probe sonicator has been developed, keeping in mind the following objectives:

- Deburring of micromilled components on soft materials like aluminium and copper, as well as hard materials like Ti-6Al-4 V and bearing steel.
- Rapid deburring to increase productivity.
- Minimisation of surface damage and collateral material removal, i.e., preserving the size and shape tolerance of the components.
- Improvement in surface finish of the components.

2. Experimental details

2.1. Ultrasonic-assisted abrasive micro-deburring setup

Fig. 1 shows the main components of the ultrasonic-assisted abrasive micro-deburring equipment. The setup consists of an ultrasonic probe sonicator (PCI Analytics, India) which has an ultrasonic transducer, a titanium horn, a temperature sensor, a height-adjustable platform for mounting the workpiece, a sound-proof enclosure, and a controller. The transducer can generate ultrasonic vibrations at a constant frequency of 20 kHz. The titanium horn was exponentially shaped (outer dia: 25 mm; tip dia: 13 mm) with the length of the exponential part being 90 mm, and can vibrate at a maximum amplitude of 35 μm at a maximum power of 750 W. Output power of the sonicator can be varied from 0 to 100 % using the controller, which in turn changes the amplitude of vibrations. The workpiece was placed in a beaker on the height-adjustable platform. A temperature sensor was provided for monitoring the process temperature, and the process can be automatically stopped when the temperature exceeds the set limit. The setup was enclosed in a sound-proof enclosure.

Table 1
Details of the deburring conditions.

Parameter	Value
Maximum power of the sonicator	750 W
Frequency	20 kHz
Base fluid for the deburring medium	deionised water
Abrasive particles used in the deburring fluid	alumina (Al_2O_3)
Mean size of the abrasives	2–5 μm
Concentration of the abrasives	3% w/v
Surfactant	sodium dodecyl sulphate (SDS)
Concentration of the surfactant	2% w/v
Work material	Aluminium 6061
Width of the microchannels	500 μm

2.2. Generation of burrs on aluminium 6061

Aluminium 6061 workpieces of dimensions 20 mm × 20 mm × 6 mm were used for the experiments. Face milling was done on both the 20 mm × 20 mm faces to maintain flatness and parallelism. Microchannels of length 5 mm were machined on the workpiece using a 0.5 mm two-fluted TiAlN coated tungsten carbide flat-end micromilling cutter (AXIS microtools, India). Cutting velocity was 10 m/min, and feed per flute was 1 μm. The depth of the microchannels were 50 μm. No cutting fluid was used during micromilling. Low cutting speed and feed were used under a dry cutting environment to generate large burrs. Fig. 2 shows the SEM image of a machined microchannel showing downmilling and upmilling burrs on the top edges of the channel. Table 1 gives details of the experimental conditions.

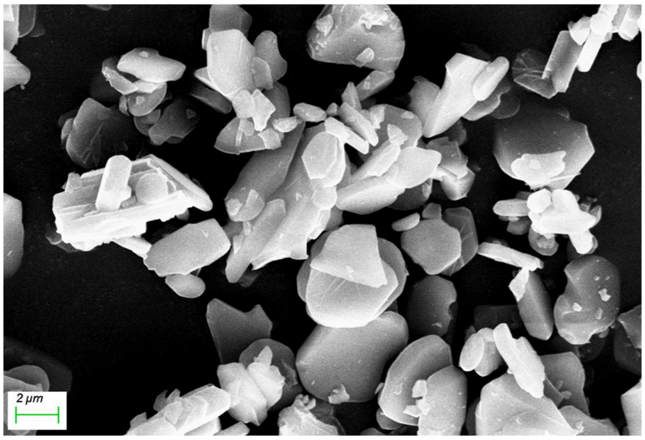

Fig. 3. SEM image of the alumina particles used in the deburring fluid.

Table 2
Details of the deburring conditions.

Parameter	Value
Power	20 %, 60 %, 100 % (at a constant SOD of 5 mm)
Amplitude (corresponding to power %)	7 μm (at 20 % power), 21 μm (at 60 % power), 35 μm (at 100 % power)
Standoff distance (SOD)	2 mm, 5 mm, 8 mm (at a constant power of 100 %)
Deburring time	50 s, in steps of 10 s
Power for pure water cavitation	100 %
SOD for pure water cavitation	2 mm

Table 3
Combination of parameters used for deburring experiments.

Sample number	Deburring fluid	Power (%)	SOD (mm)
S1	DI water	100	2
S2	DI water + 3% Al_2O_3	20	5
S3	DI water + 3% Al_2O_3	60	5
S4	DI water + 3% Al_2O_3	100	5
S5	DI water + 3% Al_2O_3	100	2
S6	DI water + 3% Al_2O_3	100	8

2.3. Preparation of the deburring fluid

The deburring fluid used in the present study is a suspension of alumina micro-particles in deionised water. Alumina micro-particles (Hindalco, India) of average particle size 2–5 μm (Fig. 3) were dispersed in deionised water at a concentration of 3% w/v and mixed in a magnetic stirrer. Disc-shaped abrasive particles were intentionally chosen for effective deburring with minimum damage to the micro-features by promoting burr removal by impact of the abrasive particles rather than micro cutting action [46]. Sodium dodecyl sulphate (SDS) was used as the surfactant at a concentration of 2% w/v to maintain the stability of the dispersion. Uniform dispersion was achieved by mixing at a constant speed of 1000 rpm for 24 h at a constant temperature of 25 °C. Larger abrasive particles or higher concentrations of abrasive would not be uniformly dispersed. Hence, the current study has used alumina abrasives with an average particle size of 2–5 μm and a concentration of 3% w/v.

2.4. Deburring experiments

Microchannels were machined on aluminium 6061, as described in section 2.2. The machined workpiece was affixed to the bottom of the beaker using two-sided adhesive tape and the beaker was then mounted on the height-adjustable platform of the deburring setup. The height of the platform was adjusted to achieve the required standoff distance (SOD) between the tip of the sonicator and the top edge of the micro-channel. The beaker was filled with the prepared deburring fluid such that the tip of the sonicator, temperature sensor, and the workpiece are completely submerged. The power of ultrasonic vibrations and the period of sonication were set as required using the controller. Power settings used were 20 %, 60 %, and 100 %. Standoff distances used were 2 mm, 5 mm, and 8 mm. One experiment was done using pure water as the deburring fluid to study the effect of pure water cavitation and to compare it with the use of abrasive fluid for deburring. Deburring parameters used are given in Table 2, and their combination is given in Table 3.

The processed samples were cleaned with acetone and dried to remove debris and residual abrasive particles. Scanning electron microscopy of the microchannels before and after deburring was performed using Zeiss Evo 18 SEM. The captured images were analysed using Zeiss AxioVision software. Areas of the burrs before and after deburring were measured to determine the extent of deburring at

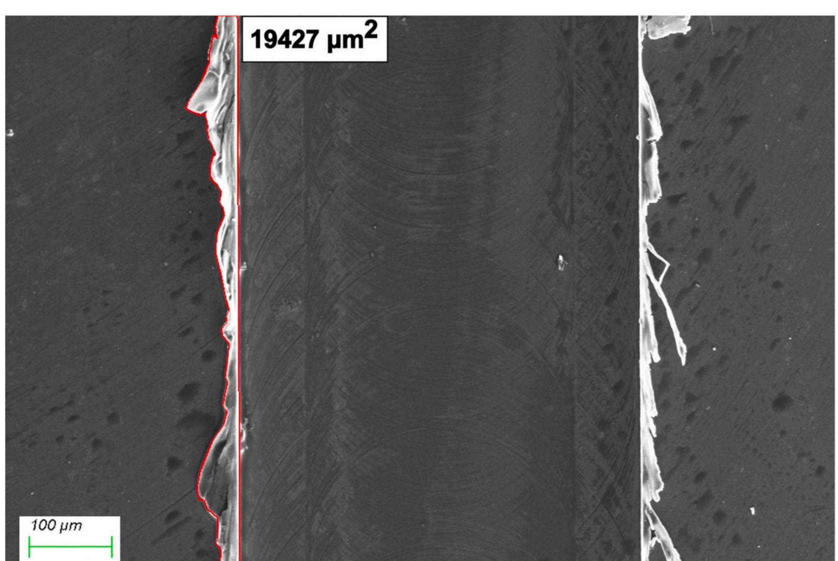

Fig. 4. A typical SEM image of a microchannel showing the measured area of the burrs on the top edge of the channel.

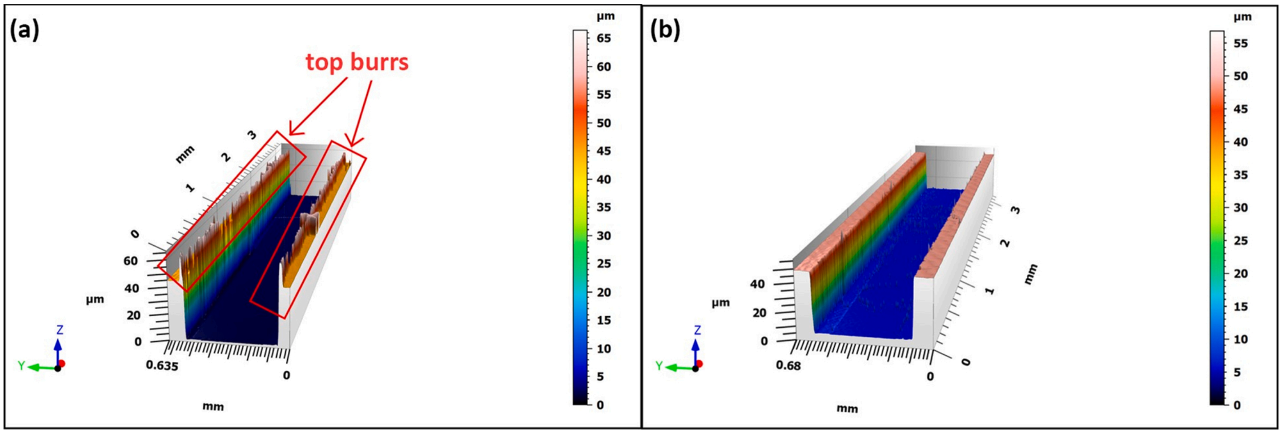

Fig. 5. 3D optical profiles of the machined microchannels: (a) before deburring, showing burrs at the top edges of the channel; (b) post deburring, the burrs are removed.

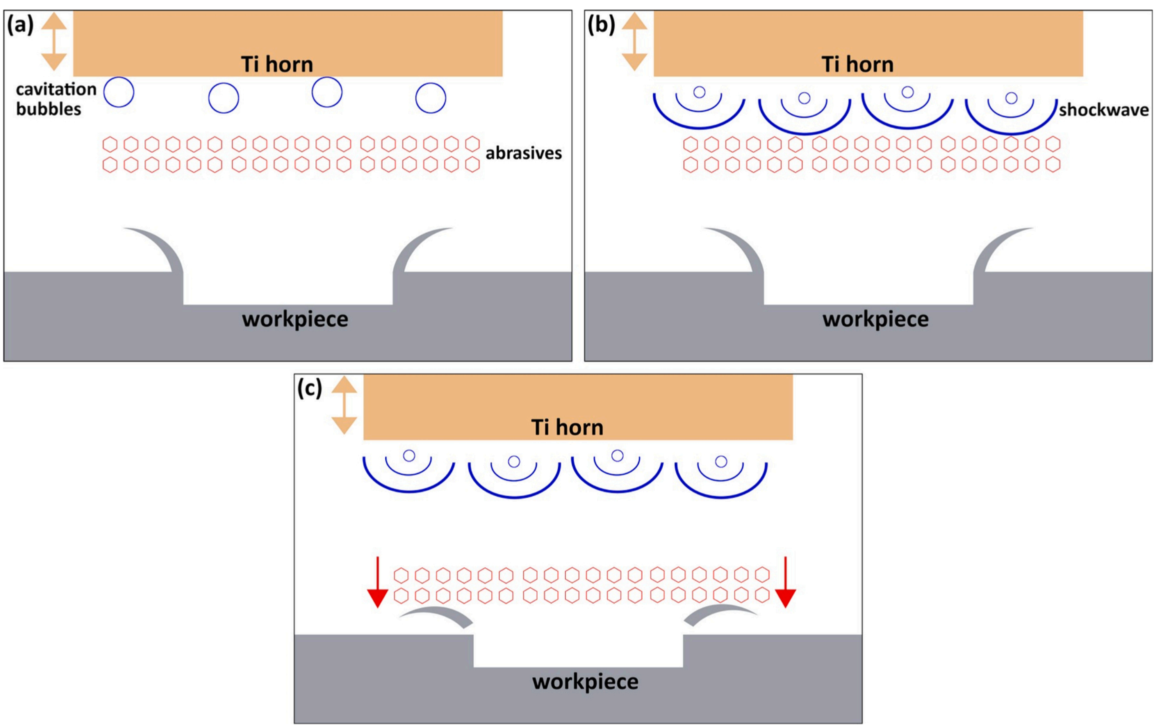

Fig. 6. Mechanism of material removal in ultrasonic vibrations assisted abrasive micro-deburring showing: (a) formation of micro cavitation bubbles; (b) generation of shockwaves by the imploding cavitation bubbles; (c) deburring by the impinging abrasive particles accelerated by the shockwaves.

various parameters. Fig. 4 shows a typical SEM image of one such microchannel. The area of burrs was measured both on the upmilling side and the downmilling side of the channel. The extent of deburring was studied after every ten seconds of processing. Surface damage caused by the abrasive particles was studied by visually inspecting the SEM images after every ten seconds of deburring.

Deburring experiments were conducted on other materials like copper, Ti-6Al-4 V alloy, and bearing steel (Power = 100 %, SOD = 2 mm). Deburring was done in steps of ten seconds until complete burr removal was achieved. SEM images of the microchannels before and after deburring were analysed to study the extent of deburring. Further, to study the mechanism of material removal in deburring, similar experiments (Power = 100 %, SOD = 2 mm) were conducted on polished aluminium surfaces for 50 s. Two such experiments were conducted, one with the workpiece held orthogonally to the axis of the sonicator, and the other with a steep angle of inclination (10° to the axis of the sonicator). SEM images of the surfaces before and after deburring were analysed to study the mechanism of material removal in deburring.

3D profiles of the microchannels before and after deburring were obtained using a non-contact optical profilometer (Taylor Hobson CCI). Fig. 5 shows the typical 3D profile of a microchannel before and after deburring. Deterioration in size and shape of the microchannels was studied by measuring the depth and width of the 3D optical profiles before and after deburring. Average surface roughness was measured at the bottom surface of the microchannels before and after deburring.

3. Results and discussion

3.1. Deburring mechanism

The mechanism of ultrasonic-assisted abrasive micro-deburring can be described as shown in Fig. 6. When the tip of the sonicator vibrates in

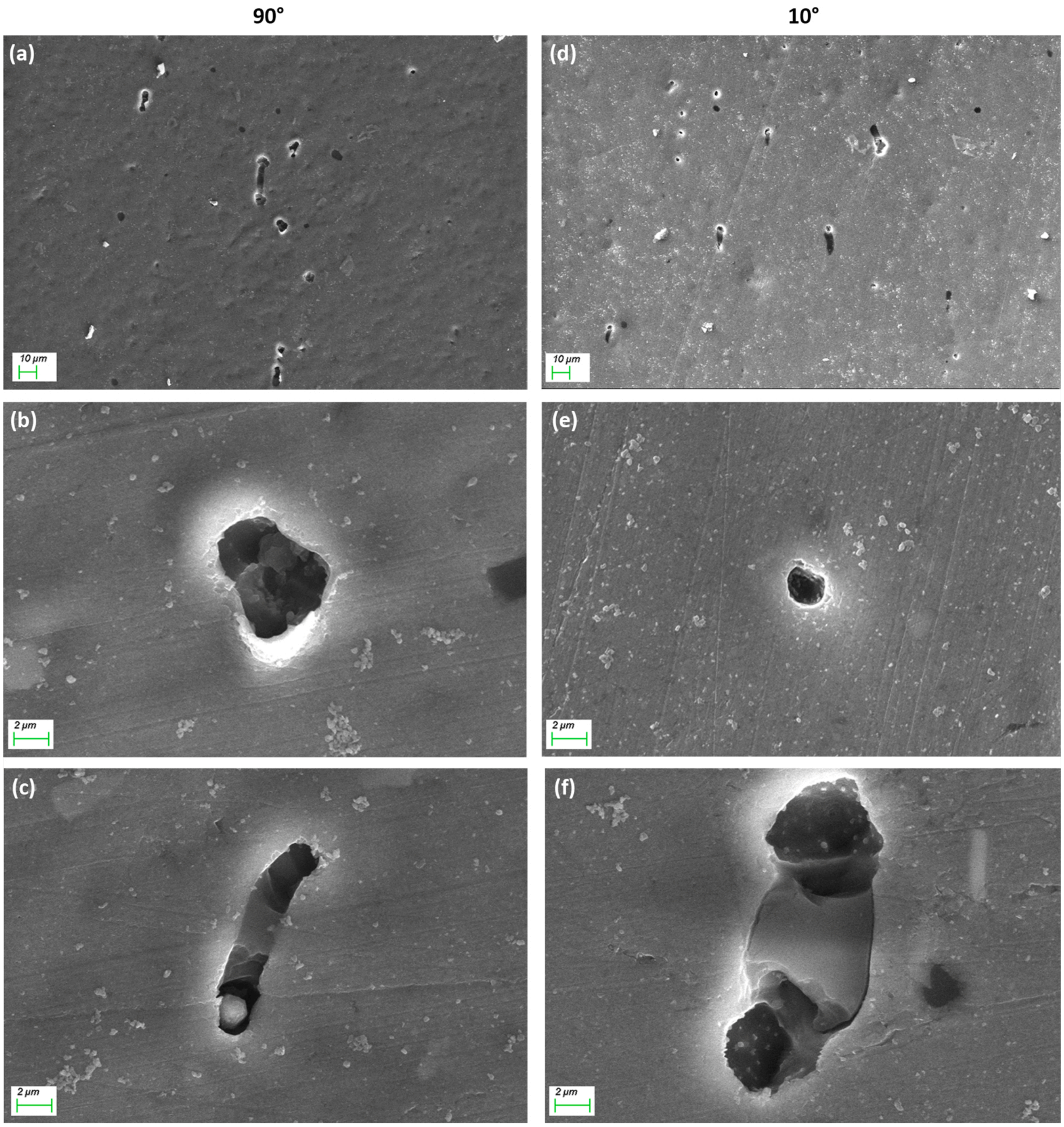

Fig. 7. Deburring test conducted on polished aluminium surfaces to determine the mechanism of material removal: (a) impact craters formed on the surface by orthogonal impingement; (b) hemispherical type craters on (a); (c) elongated impact crater on (a); (d) impact craters formed by inclined impingement; (e) hemispherical type craters on (d); (f) elongated impact crater on (d).

the liquid medium, compression and rarefaction cycles give rise to high and low local pressures. When the pressure difference between the high- and low-pressure cycles is sufficiently high, cavitation bubbles are formed from the dissolved gases or vapour, as shown in Fig. 6a [47]. These cavitation bubbles increase in size and collapse violently in the successive compression cycles, creating high-pressure shockwaves, as shown in Fig. 6b [43,47–50]. Shockwaves generated from the collapsing bubbles accelerate the abrasive particles towards the surface of the workpiece [51], and the accelerated abrasives break away the burrs by impact, as shown in Fig. 6c.

To study the role of abrasive particles in deburring, tests were conducted on polished aluminium surfaces as described in the experimental details (SOD = 2 mm, Power = 100 %). Two such experiments were conducted, one with the direction of impingement orthogonal to the surface of the workpiece and the other with the direction of impingement steeply inclined to the surface of the workpiece (10°). SEM images of the surfaces are shown in Fig. 7. Crater-like surface damage was found in both orthogonal and inclined impingement cases. Further, craters that appear to be of elongated nature were also found on the surfaces (Fig. 7c and f). The presence of damage craters indicates that material is removed by the impact of the accelerating abrasives. No micro-cutting action was observed in the SEM images of the surfaces. Bitter [52,53] and Finnie et al. [54] have studied the erosion phenomena of abrasives at different incidence angles. They have concluded that near-normal incidence produces more impact while low incidence angle produces micro cutting action. Hashish [55] has also reported that the removal of material is by impact or plastic deformation at near orthogonal impingement in abrasive water jet machining. Based on these observations, it can be safely inferred that the deburring mechanism is by impact of the abrasive particles.

3.2. Burr reduction and surface damage

Fig. 8 shows the SEM images of the microchannels on aluminium

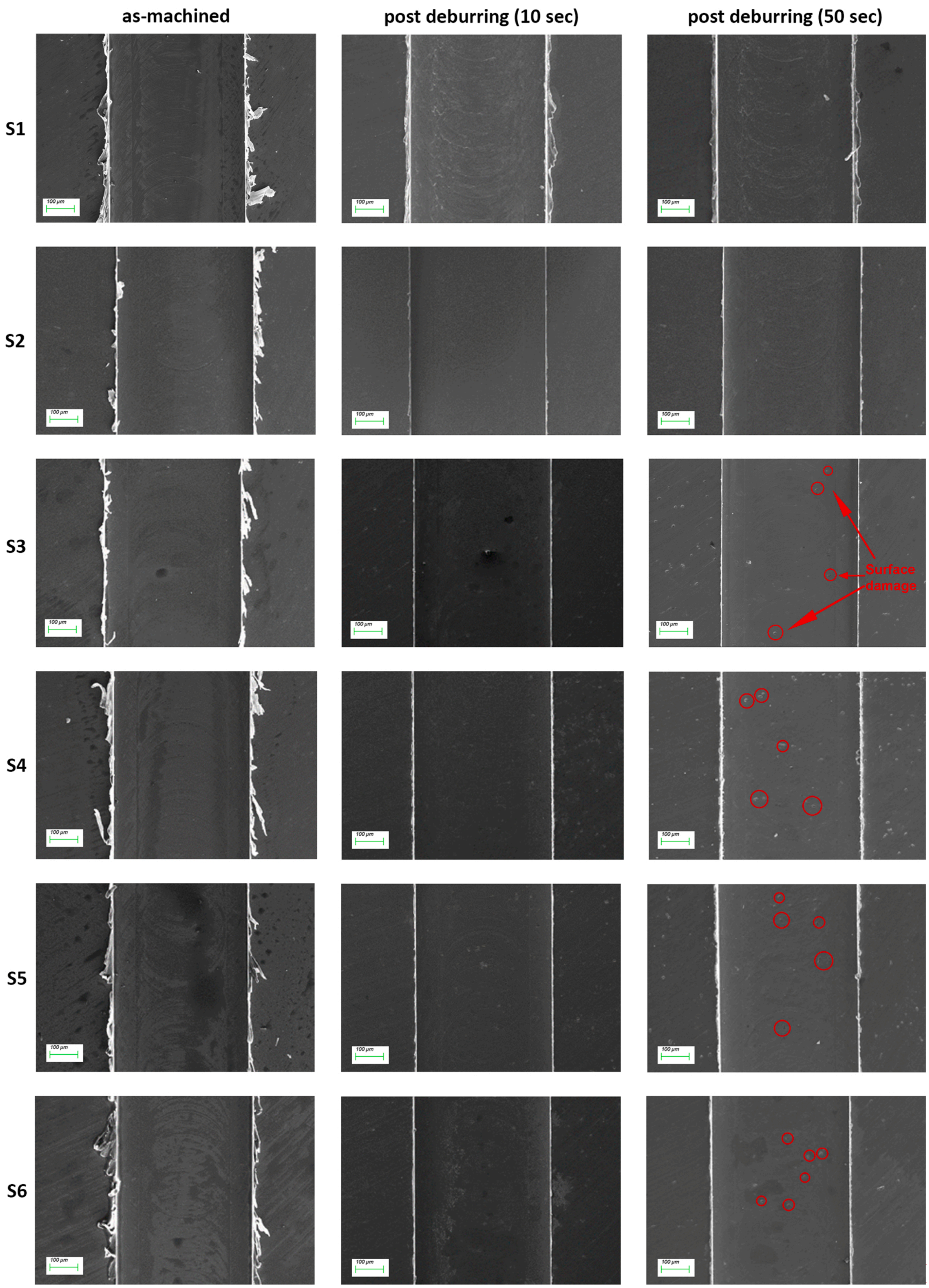

Fig. 8. SEM photographs of microchannels before deburring and post deburring at different parameters showing the progress of burr removal and surface damage. No surface damage was observed on any of the samples after 10 s but, after 50 s, surface damage was visible on samples S3, S4, S5, and S6.

before deburring, after ten seconds, and after 50 s of deburring. Sample S1 was processed with pure water as the deburring fluid, and samples S2 to S6 were processed with abrasive fluid with parameters as given in Table 3. In all the cases, maximum possible burr removal was achieved within the first ten seconds. It can be seen that after 50 s of deburring, the amount of material removed is not significant. It can be observed from the SEM images that pure water cavitation has not resulted in significant deburring of the microchannels, whereas the addition of

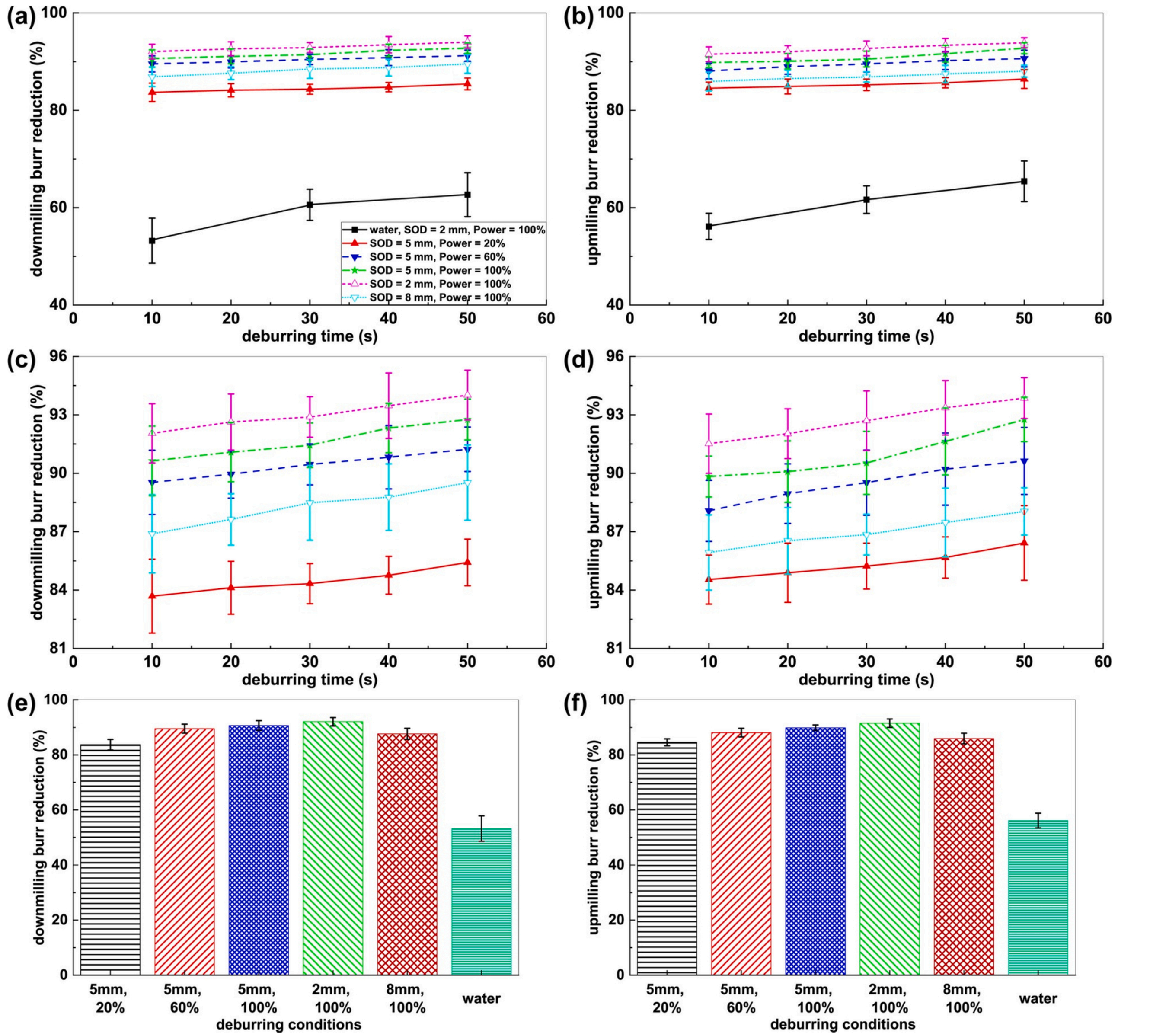

Fig. 9. Percentage of burrs removed shown at various parameters: (a) downmilling side; (b) upmilling side; (c) close up view of (a); (d) close up view of (b); (e) downmilling side after 10 s; (f) upmilling side after 10 s. Burr removal was minimal in the case of pure water cavitation (S1). In case of abrasive deburring, the amount of burr removal increased with increasing power and decreasing standoff distance.

abrasive particles has quite increased the extent of deburring. This leads to an observation that the accelerated abrasive particles play a significant role in the deburring mechanism. The extent of burr reduction after a deburring time is calculated using Eq. 1. The area of the burrs was measured by analysing the SEM images of the microchannels before and after deburring. Volumetric burr reduction could not be reliably measured because the actual measurement of burr reduction by weighing was not very effective as the mass loss due to deburring was very small compared to the mass of the component. In the present study, area measurement provided more reliable data.

$$burrreduction(\%) = \frac{A_0 - A_t}{A_0} \times 100 \quad (1)$$

where A_0 is the area of burrs on the as-machined microchannels and A_t is the area of burrs on microchannels after deburring for a time t.

The extent of deburring for both upmilling and downmilling burrs on aluminium is plotted in Fig. 9. The role of abrasive particles in deburring is evident as observed in the SEM images in Fig. 8. It is also observed that most of the deburring is completed within the first ten seconds (> 80 % burr reduction), as shown in Fig. 9. This is a significant improvement over pure water ultrasonic cavitation based deburring methods in literature, which reported a deburring time of 30 min to a few hours [41,42,44,56,57]. Yeo et al. [41] have reported a deburring time of around seven minutes for an aluminium specimen employing a bath sonicator. Pure water cavitation has not played a significant role in deburring in the present study, and complete deburring could not be achieved even after 50 s for soft material like aluminium. For example, Khmelev et al. [44] have reported a deburring time of five hours for soft material like brass using ultrasonic cavitation in an ultrasonic bath. They have further reported that by adding abrasive particles, deburring time can be brought down to 60 min. In the present study, by employing a probe sonicator, deburring is achieved in a significantly shorter time as compared to past studies. This can be attributed to the focusing of cavitation energy at a particular region of interest, which has significantly reduced the deburring time. The extent of deburring for all cases up to ten seconds is shown in Fig. 9. It can be seen that for the sample S5

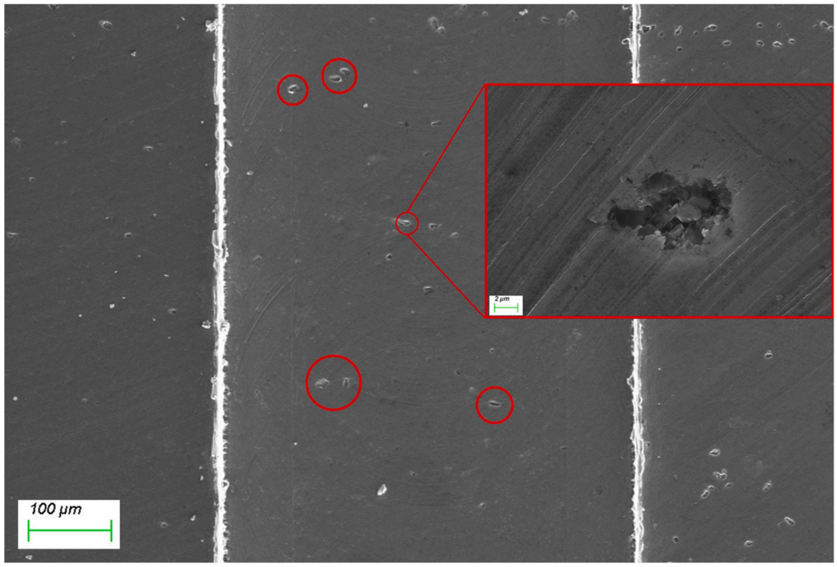

Fig. 10. Magnified view of the surface of the microchannel on sample S5 showing crater-like surface damage (shown in the inset) after 50 s of deburring.

Table 4
Impact craters formed by grits at different parameters after 10 and 50 s of deburring.

Sample number	Parameters	No.of craters (10 s) (/mm2)	No.of craters (50 s) (/mm2)
S1	pure water, power = 100 %, SOD = 2 mm	–	–
S2	power = 20 %, SOD = 5 mm	5 ± 2	35 ± 7
S3	power = 60 %, SOD = 5 mm	18 ± 3	77 ± 5
S4	power = 100 %, SOD = 5 mm	23 ± 3	157 ± 13
S5	power = 100 %, SOD = 2 mm	31 ± 7	180 ± 17
S6	power = 100 %, SOD = 8 mm	26 ± 6	122 ± 8

(SOD = 2 mm and Power = 100 %), burr reduction is the highest (down milling burr reduction = 92 %; up milling burr reduction = 91.5 %). It can be seen that the extent of deburring increases with an increase in power (S2, S3, S4 in this order) and with a decrease in standoff distance (S5, S4, S6 in this order).

It has been observed in Fig. 8 that after prolonged deburring, surface damage through crater formation has occurred by the impinging abrasive particles. Damage craters were observed on the surfaces of microchannels after 50 s of deburring, while no such damages were seen after 10 s of deburring. Fig. 10 shows a magnified view of the damage craters on sample S5 after 50 s of deburring. The number of craters formed by abrasive impact was measured from the SEM images of the channels post deburring and tabulated in Table 4. Deburring for prolonged durations has been found to increase the surface damage without significantly increasing the extent of burr reduction. It can be inferred that significant burr reduction can be achieved in ten seconds while keeping the surface damage to a minimum level.

Deburring experiments were conducted on other materials like copper, Ti-6Al-4 V, and bearing steel to assess the feasibility of the present deburring process. Fig. 11 shows the SEM images of burrs on these materials, and Fig. 12 shows the time-based burr reduction. It can be seen that the deburring process has been able to remove burrs completely on copper in ten seconds. In case of Ti-6Al-4 V and bearing steel, complete deburring took longer than aluminium and copper (3 min for Ti-6Al-4 V and more than 6 min for bearing steel), and a very less amount of burrs were removed in ten seconds as shown by the SEM images. Deburring time for different work materials can be correlated to their mechanical properties, particularly the impact strength. Some of the mechanical properties are given in Table 5.

3.3. Deterioration in size and shape tolerances

Fig. 13 shows the 3D cross-section profiles of the microchannels on Al 6061 before deburring and after 50 s of deburring obtained from the 3D optical profilometer. It is observed that the variation in height of the microchannels is less than 0.25 % at the most, and no change in width was observed, indicating that the size and shape tolerances of the samples are preserved. This is attributed to the disc shape of the chosen abrasive grits. The present deburring process is much effective in preserving the dimensional tolerances of the components while keeping the deburring time an order of magnitude lower as compared to past studies including ultrasonic deburring [45], abrasive peening [41,43], micro-EDM [32], or laser-based process [5,38]. The absence of burrs at the top edge of the microchannels post deburring is also observed in all the cases using abrasive fluid. Burrs were still present post deburring in case of pure water cavitation.

3.4. Surface finish

Fig. 14a shows the variations in average surface roughness at the bottom surface of the microchannels with deburring time. For pure water cavitation, surface roughness after 50 s of deburring does not decrease significantly (as shown in Fig. 14a and b). This is because cavitation energy does not cause any micro-polishing action of the surface. Further, the surface roughness has decreased in cases where abrasives were used. Surface roughness has decreased from 8.97 nm to as low as 6.63 nm post deburring, resulting in a 26 % improvement in surface finish. This is due to the material removal action of the abrasive particles, although no micro-polishing effect was evident from the SEM images of the processed surfaces. From Fig. 14a, it is observed that the average surface roughness decreases up to 40 s of deburring and then it increases at 50 s. This can be attributed to the increased damage craters after 50 s of deburring, leading to a deterioration of surface quality. It is observed that sample S5 (SOD = 2 mm, Power = 100 %) shows the highest reduction in surface roughness. Further, surface roughness has been observed to decrease with an increase in power and a decrease in standoff distance.

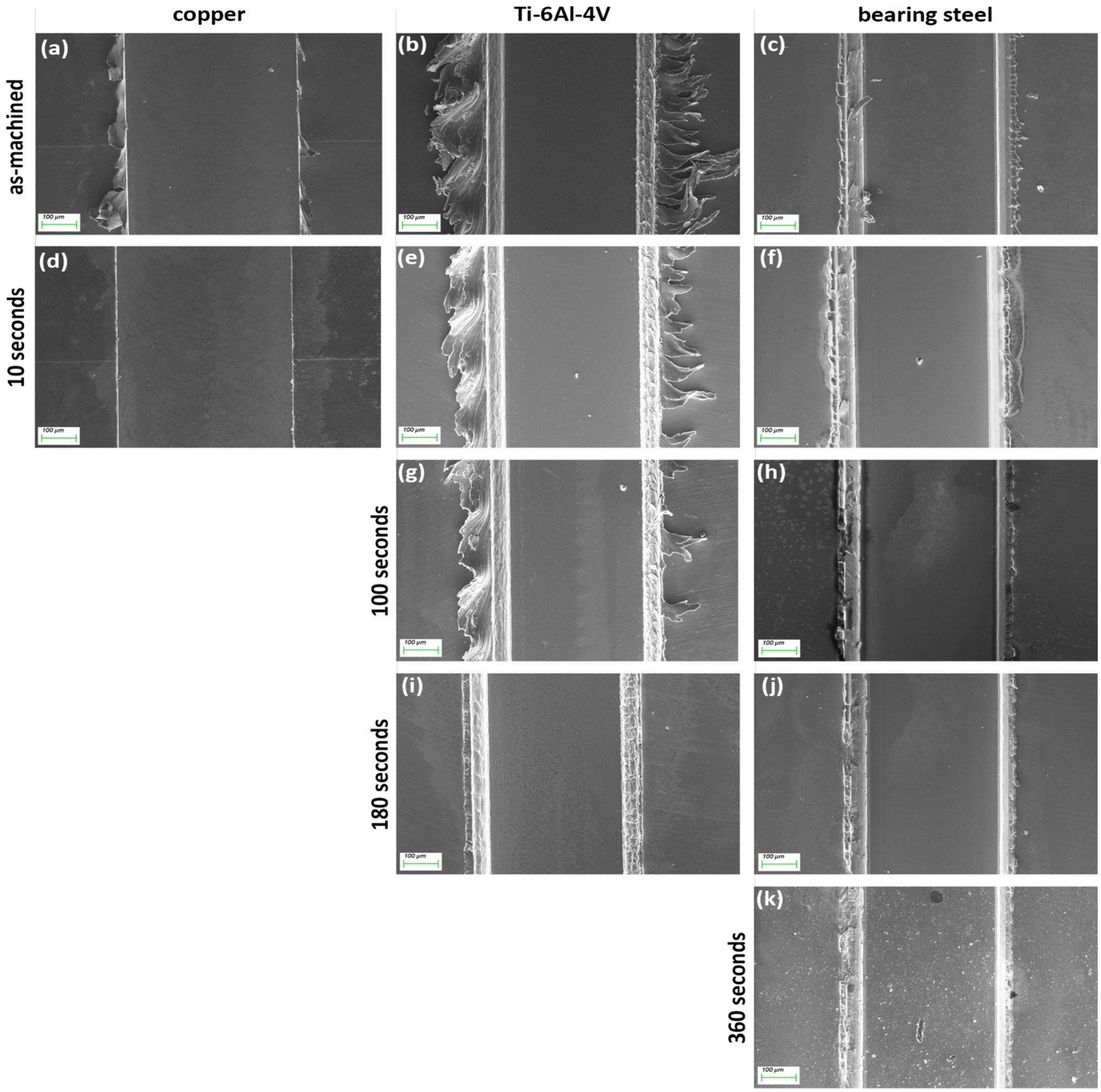

Fig. 11. SEM images of microchannels before and after deburring on other materials (SOD = 2 mm, Power = 100 %): (a) copper before deburring; (b) Ti-6Al-4 V before deburring; (c) bearing steel before deburring; (d) copper after 10 s of deburring (complete deburring); (e) Ti-6Al-4 V after 10 s; (f) bearing steel after 10 s; (g) Ti-6Al-4 V after 100 s; (h) Bearing steel after 100 s; (i) Ti- Al-4 V after 180 s (complete deburring); (j) Bearing steel after 180 s; (k) Bearing steel after 360 s (maximum deburring).

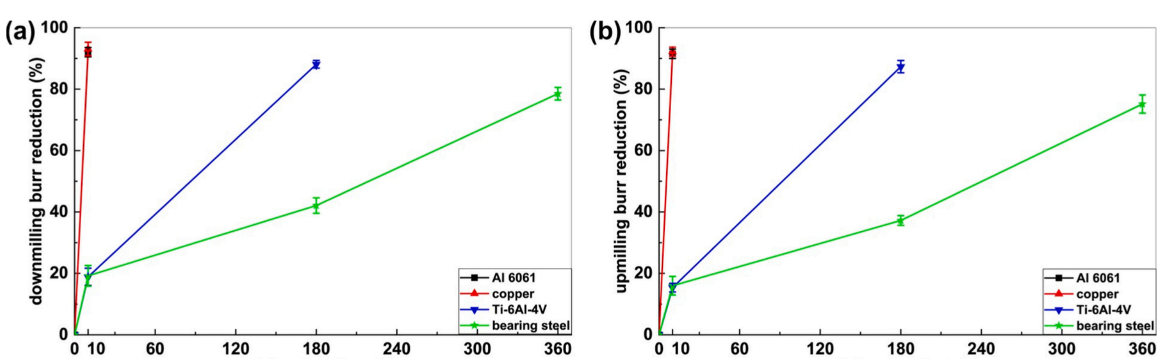

Fig. 12. Percentage of burrs removed with time for Al 6061, copper, Ti-6Al-4 V, and bearing steel (SOD = 2 mm, Power = 100 %): (a) downmilling side; (b) upmilling side.

Table 5
Mechanical properties of work materials [58–63].

	UTS (MPa)	Yield strength (MPa)	Charpy impact energy (J)
Al 6061	318	276	10 – 18
Copper	290	180 – 220	8 – 12
Ti-6Al-4V	954	729	34
Bearing steel	2250	1410	53

4. Conclusions

In the present study, an ultrasonic-assisted abrasive micro-deburring process is developed employing a probe sonicator and is applied for deburring micromilled channels on Al 6061, copper, Ti-6Al-4 V, and bearing steel. The following conclusions are made:

- The mechanism of deburring is mainly by the impact of abrasive particles accelerated by shockwaves generated by the collapsing ultrasonic cavitation bubbles.
- Maximum significant burr removal has been achieved in a short time, i.e., a burr reduction of 92 % was observed in ten seconds for soft materials like Al 6061 and copper, and within three to six minutes for hard materials like Ti-6Al-4 V and bearing steel.
- The extent of deburring can be correlated to the mechanical properties of the work materials, particularly the impact strength. Similarly, the time required for deburring is inversely related to the impact strength of the work material.
- Maximum deburring can be achieved by using higher power and a smaller standoff distance between the horn and the workpiece.
- Deterioration in size and shape tolerance was minimal in all the parameters of deburring, the maximum change in size of the microchannels observed was around 0.25 %
- Increasing the deburring time increases surface damage without significantly increasing the extent of burrs removed.
- Surface roughness has decreased from 8.97 nm to as low as 6.63 nm post deburring, resulting in a 26 % improvement in surface finish. This is due to the material removal action of the abrasive particles, though no micro-polishing effect was evident from the SEM images.
- Surface roughness of the channels reduced initially with deburring time and then increased. This is due to the increased surface damage from the impinging abrasive particles due to prolonged deburring.

Funding sources

This research did not receive any specific grant from funding agencies in the public, commercial, or not-for-profit sectors.

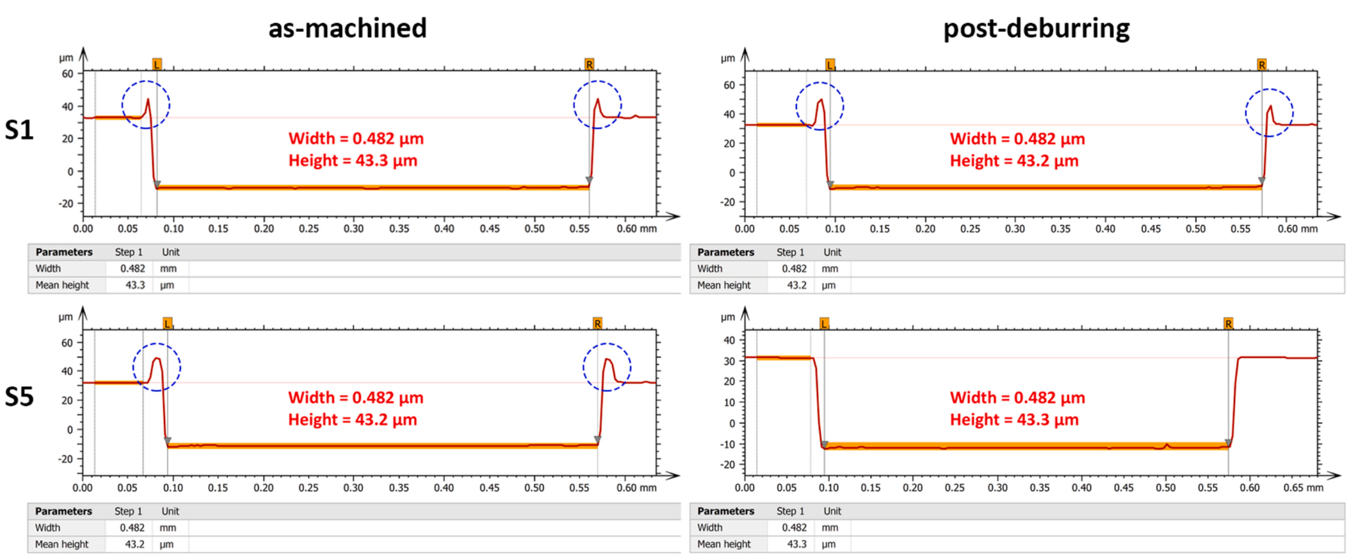

Fig. 13. Cross-section profiles of the microchannels before and after deburring for 50 s showing the size and shape tolerance at different parameters. Burrs were still present in case of pure water cavitation (as shown in S1 post deburring), whereas no burrs were present in case of abrasive fluid (sample S5). The size and shape tolerance of the samples is also preserved after deburring.

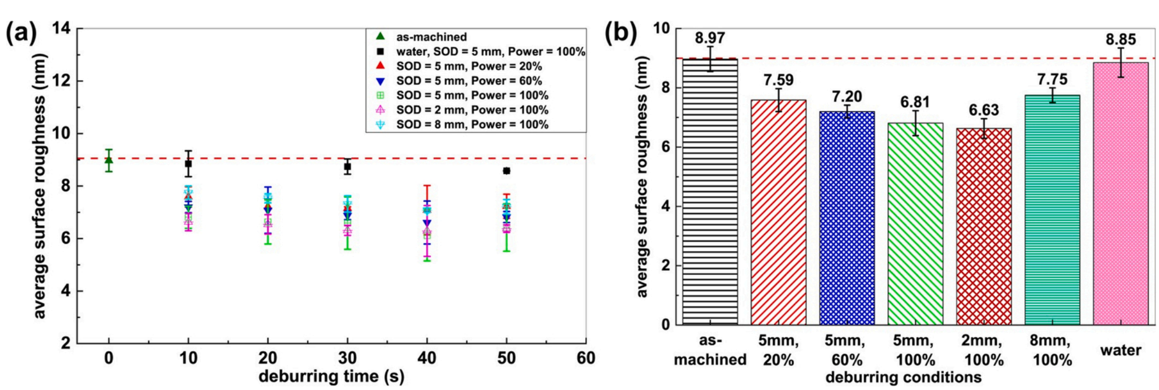

Fig. 14. Cross-section profiles of the microchannels before and after deburring for 50 s showing the size and shape tolerance at different parameters. Burrs were still present in case of pure water cavitation (as shown in S1 post deburring), whereas no burrs were present in case of abrasive fluid (sample S5). The size and shape tolerance of the samples is also preserved after deburring.

Declaration of Competing Interest

The authors report no declarations of interest.

Appendix A. Supplementary data

Supplementary material related to this article can be found, in the online version, at doi:https://doi.org/10.1016/j.jmapro.2021.04.019.

References

[1] Ko S-L, Dornfeld DA. A study on burr formation mechanism. J Eng Mater Technol 1991;113:75–87. https://doi.org/10.1115/1.2903385.
[2] Lee K, Dornfeld DA. Micro-burr formation and minimization through process control. Precis Eng 2005;29:246–52. https://doi.org/10.1016/j.precisioneng.2004.09.002.
[3] DeVor R, Ehmann K, Kapoor S. Technology assessment on current advanced research in micro-machining and related areas. McLean, VA, USA: The Association For Manufacturing Technology; 2004. p. 239.
[4] Bissacco G, Hansen HN, De Chiffre L. Micromilling of hardened tool steel for mould making applications. J Mater Process Technol 2005;167:201–7. https://doi.org/10.1016/j.jmatprotec.2005.05.029.
[5] Lee SH, Dornfeld DA. Precision laser deburring. J Manuf Sci Eng 2001;123:601. https://doi.org/10.1115/1.1381007.
[6] Pekelharing A. The exit angle failure in interrupted cutting. Ann CIRP 1978;27:5.
[7] Nakayama K, Arai M. Burr formation in metal cutting. CIRP Ann Manuf Technol 1987;36:33–6. https://doi.org/10.1016/S0007-8506(07)62547-5.
[8] Aurich JC, Dornfeld D, Arrazola PJ, Franke V, Leitz L, Min S. Burrs—analysis, control and removal. CIRP Ann Manuf Technol 2009;58:519–42. https://doi.org/10.1016/j.cirp.2009.09.004.
[9] Chern G-L, Dornfeld DA. Burr/Breakout model development and experimental verification. J Eng Mater Technol 1996;118:201–6. https://doi.org/10.1115/1.2804887.
[10] Hashimura M, Chang Y, Dornfeld D. Analysis of burr formation mechanism in orthogonal cutting. ASME is J Manuf Sci Eng 1999;121:1–7. https://doi.org/10.1115/1.2830569.
[11] Hashimura M, Hassamontr J, Dornfeld DA. Effect of in-plane exit angle and rake angles on burr height and thickness in face milling operation. J Manuf Sci Eng 1999;121:13–9. https://doi.org/10.1115/1.2830566.
[12] Niknam SA, Songmene V. Milling burr formation, modeling and control: a review. Proc Inst Mech Eng Part B J Eng Manuf 2015;229:893–909. https://doi.org/10.1177/0954405414534827.
[13] Min S, Dornfeld DA, Kim J, Shyu B. Finite element modeling of burr formation in metal cutting. Mach Sci Technol 2001;5:307–22. https://doi.org/10.1081/MST-100108617.
[14] Gillespie LK. Burrs produced by end milling. Kansas City, Mo. (USA): Bendix Corp.; 1976. https://doi.org/10.2172/7259917.
[15] Chang SSF, Bone GM. Burr size reduction in drilling by ultrasonic assistance. Robot Comput Integr Manuf 2005;21:442–50. https://doi.org/10.1016/j.rcim.2004.11.005.
[16] Kim J, Min S, Dornfeld DA. Optimization and control of drilling burr formation of AISI 304L and AISI 4118 based on drilling burr control charts. Int J Mach Tools Manuf 2001;41:923–36. https://doi.org/10.1016/S0890-6955(00)00131-0.
[17] Tripathi S, Dornfeld DA. Review of geometric solutions for milling burr prediction and minimization. Proc Inst Mech Eng Part B J Eng Manuf 2006;220:459–66. https://doi.org/10.1243/095440505X32652.
[18] Chen M, Liu G, Shen Z. Study on active process control of burr formation in Al-alloy milling process. 2006 IEEE International Conference on Automation Science and Engineering 2006:431–6. https://doi.org/10.1109/COASE.2006.326920.
[19] Lee K, Dornfeld DA. An experimental study on burr formation in micro-milling aluminium and copper. Transactions of NAMRI/SME 2002:1–8.
[20] Filiz S, Conley CM, Wasserman MB, Ozdoganlar OB. An experimental investigation of micro-machinability of copper 101 using tungsten carbide micro-endmills. Int J Mach Tools Manuf 2007;47:1088–100. https://doi.org/10.1016/j.ijmachtools.2006.09.024.
[21] Kumar AS, Deb S, Paul S. A study on micro-milling of aluminium 6061 and copper with respect to cutting forces. Surface roughness and burr formation, Volume 4. Processes, College Station, Texas, USA: American Society of Mechanical Engineers; 2018. https://doi.org/10.1115/MSEC2018-6570. p. V004T03A014.
[22] Hassanpour H, Sadeghi MH, Rezaei H, Rasti A. Experimental study of cutting force, microhardness, surface roughness, and Burr size on micromilling of Ti6Al4V in minimum quantity lubrication. Mater Manuf Process 2016;31:1654–62. https://doi.org/10.1080/10426914.2015.1117629.
[23] Vazquez E, Gomar J, Ciurana J, Rodríguez CA. Analyzing effects of cooling and lubrication conditions in micromilling of Ti6Al4V. J Clean Prod 2015;87:906–13. https://doi.org/10.1016/j.jclepro.2014.10.016.
[24] Lee K, Stirn B, Dornfeld DA. Burr formation in micro-machining aluminum, 6061-T6. In: Inasaki I, editor. Initiatives of Precision Engineering at the Beginning of a Millennium: 10th International Conference on Precision Engineering (ICPE) July 18–20, 2001; 2002. p. 47–51. https://doi.org/10.1007/0-306-47000-4_8.
[25] Kumar P, Kumar M, Bajpai V, Singh NK. Recent advances in characterization, modeling and control of burr formation in micro-milling. Manuf Lett 2017;13:1–5. https://doi.org/10.1016/j.mfglet.2017.04.002.
[26] Saptaji K, Subbiah S. Burr reduction of micro-milled microfluidic channels mould using a tapered tool. Procedia Eng 2017;184:137–44. https://doi.org/10.1016/j.proeng.2017.04.078.
[27] Ni C, Zhu L, Liu C, Yang Z. Analytical modeling of tool-workpiece contact rate and experimental study in ultrasonic vibration-assisted milling of Ti–6Al–4V. Int J Mech Sci 2018;142–143:97–111. https://doi.org/10.1016/j.ijmecsci.2018.04.037.
[28] Liu Q, Xu J, Yu H. Experimental study of tool wear and its effects on cutting process of ultrasonic-assisted milling of Ti6Al4V. Int J Adv Manuf Technol 2020;108:2917–28. https://doi.org/10.1007/s00170-020-05593-3.
[29] Rinck PM, Gueray A, Kleinwort R, Zaeh MF. Experimental investigations on longitudinal-torsional vibration-assisted milling of Ti-6Al-4V. Int J Adv Manuf Technol 2020;108:3607–18. https://doi.org/10.1007/s00170-020-05392-w.
[30] Jin SY, Pramanik A, Basak AK, Prakash C, Shankar S, Debnath S. Burr formation and its treatments—a review. Int J Adv Manuf Technol 2020;107:2189–210. https://doi.org/10.1007/s00170-020-05203-2.
[31] Aurich JC, Kirsch B, Setti D, Axinte D, Beaucamp A, Butler-Smith P, et al. Abrasive processes for micro parts and structures. CIRP Ann Manuf Technol 2019;68:653–76. https://doi.org/10.1016/j.cirp.2019.05.006.
[32] Jeong YH, HanYoo B, Lee HU, Min B-K, Cho D-W, Lee SJ. Deburring microfeatures using micro-EDM. J Mater Process Technol 2009;209:5399–406. https://doi.org/10.1016/j.jmatprotec.2009.04.021.
[33] Mathai G, Melkote S. Effect of process parameters on the rate of abrasive assisted brush deburring of microgrooves. Int J Mach Tools Manuf 2012;57:46–54. https://doi.org/10.1016/j.ijmachtools.2012.02.007.
[34] Liao L, (Jeff) Xi F, Liu K. Modeling and control of automated polishing/deburring process using a dual-purpose compliant toolhead. Int J Mach Tools Manuf 2008;48:1454–63. https://doi.org/10.1016/j.ijmachtools.2008.04.009.
[35] Malayath G, KN J, Sidpara AM, Deb S. Experimental and theoretical investigation into simultaneous deburring of microchannel and cleaning of the cutting tool in micromilling. Proc Inst Mech Eng Part B J Eng Manuf 2018:095440541879886. https://doi.org/10.1177/0954405418798864.
[36] Okada A, Yonehara H, Okamoto Y. Fundamental study on micro-deburring by large-area EB irradiation. Procedia CIRP 2013;5:19–24. https://doi.org/10.1016/j.procir.2013.01.004.
[37] Balasubramaniam R, Krishnan J, Ramakrishnan N. Investigation of AJM for deburring. J Mater Process Technol 1998;79:52–8. https://doi.org/10.1016/s0924-0136(97)00305-1.
[38] Chang W, Luo X, Ritchie JM, Sun J, Mack C. Laser deburring process for structured edges on precision moulds. Int J Nanomanuf 2011;7:327–35. https://doi.org/10.1504/IJNM.2011.042470.
[39] Hesson JR. Fundamentals of ultrasonic cleaning. Saatavissa. 2003. Http://WwwHessonicCom/Fundamentals-of-Ultrasonic-CleaningHtml[Viitattu8112015].
[40] Suslick KS, Nyborg WL. Ultrasound: its chemical, physical and biological effects. 1990. https://doi.org/10.1121/1.398864.
[41] Yeo SH, BBKA Ngoi, Chua LY. Ultrasonic deburring. Int J Adv Manuf Technol 1997;13:333–41. https://doi.org/10.1007/BF01178253.
[42] Ch Horsch, Schulze V, Löhe D. Deburring and surface conditioning of micro milled structures by micro peening and ultrasonic wet peening. Microsyst Technol 2006;12:691–6. https://doi.org/10.1007/s00542-006-0087-1.
[43] Kienzler A, Deuchert M, Schulze V. Burr minimization and removal by micro milling strategies or micro peening processes. In: Aurich JC, Dornfeld D, editors. Burrs - analysis, control and removal. Berlin, Heidelberg: Springer Berlin Heidelberg; 2010. p. 237–43. https://doi.org/10.1007/978-3-642-00568-8_26.
[44] Khmelev VN, Tsyganok SN, Kuzovnikov YM, Shakura VA, Khmelev MV, Zorin SS. Study of ultrasonic cavitation action on the process of part cleaning from burrs. 2016 17th International Conference of Young Specialists on Micro/Nanotechnologies and Electron Devices (EDM) 2016:275–9. https://doi.org/10.1109/EDM.2016.7538740.
[45] Choi HZ, Lee SW, Kim GH, Choi YJ, Ko S-L. Micro deburring technology using ultrasonic vibration with abrasive. 2004.
[46] Hutchings IM. A model for the erosion of metals by spherical particles at normal incidence. Wear 1981;70:269–81. https://doi.org/10.1016/0043-1648(81)90347-1.
[47] Tsochatzidis NA, Guiraud P, Wilhelm AM, Delmas H. Determination of velocity, size and concentration of ultrasonic cavitation bubbles by the phase-Doppler technique. Chem Eng Sci 2001;56:1831–40. https://doi.org/10.1016/s0009-2509(00)00460-7.
[48] Lauterborn W, Ohl C-D. Cavitation bubble dynamics. Ultrason Sonochem 1997;4:65–75. https://doi.org/10.1016/S1350-4177(97)00009-6.
[49] van Wijngaarden L. Mechanics of collapsing cavitation bubbles. Ultrason Sonochem 2016;29:524–7. https://doi.org/10.1016/j.ultsonch.2015.04.006.
[50] Beaucamp A, Katsuura T, Kawara Z. A novel ultrasonic cavitation assisted fluid jet polishing system. CIRP Ann Manuf Technol 2017;66:301–4. https://doi.org/10.1016/j.cirp.2017.04.083.
[51] Poulain S, Guenoun G, Gart S, Crowe W, Jung S. Particle motion induced by bubble cavitation. Phys Rev Lett 2015;114:214501. https://doi.org/10.1103/PhysRevLett.114.214501.
[52] Bitter JGA. A study of erosion phenomena part I. Wear 1963;6:5–21. https://doi.org/10.1016/0043-1648(63)90003-6.
[53] Bitter JGA. A study of erosion phenomena. Wear 1963;6:169–90. https://doi.org/10.1016/0043-1648(63)90073-5.
[54] Finnie I, Stevick GR, Ridgely JR. The influence of impingement angle on the erosion of ductile metals by angular abrasive particles. Wear 1992;152:91–8. https://doi.org/10.1016/0043-1648(92)90206-N.
[55] Hashish M. A modeling study of metal cutting with abrasive waterjets. J Eng Mater Technol 1984;106:88–100. https://doi.org/10.1115/1.3225682.

[56] Toh CK. The use of ultrasonic cavitation peening to improve micro-burr-free surfaces. Int J Adv Manuf Technol 2006;31:688–93. https://doi.org/10.1007/s00170-005-0249-9.

[57] Khmelev VN, Tsyganok SN, Romashkin AA, Titov GA. Deburring of small parts in hard-to-reach places by ultrasonic action. 2013 14th International Conference of Young Specialists on Micro/Nanotechnologies and Electron Devices 2013:176–81. https://doi.org/10.1109/EDM.2013.6641968.

[58] Niinomi M. Mechanical properties of biomedical titanium alloys. Mater Sci Eng A 1998;243:231–6. https://doi.org/10.1016/S0921-5093(97)00806-X.

[59] Li M, Zinkle SJ. Physical and mechanical properties of copper and copper alloys. Comprehensive nuclear materials. Elsevier; 2012. p. 667–90. https://doi.org/10.1016/B978-0-08-056033-5.00122-1.

[60] Chakraborty J, Bhattacharjee D, Manna I. Austempering of bearing steel for improved mechanical properties. Scr Mater 2008;59:247–50. https://doi.org/10.1016/j.scriptamat.2008.03.023.

[61] Lumley RN, Polmear IJ, Morton AJ. Development of mechanical properties during secondary aging in aluminium alloys. Mater Sci Technol 2005;21:1025–32. https://doi.org/10.1179/174328405X51875.

[62] Lee D-G, Lee S, Lee Y. Effect of precipitates on damping capacity and mechanical properties of Ti–6Al–4V alloy. Mater Sci Eng A 2008;486:19–26. https://doi.org/10.1016/j.msea.2007.08.053.

[63] Ali MB, Zakaria KA, Abdullah S, Alkhari MR. Correlation of impact energy from instrumented charpy impact. AMM 2015;815:221–6. https://doi.org/10.4028/www.scientific.net/AMM.815.221.